Ab initio calculation of ideal strength and phonon instability of graphene under tension

Fang Liu
School of Applied Mathematics, Central University of Finance and Economics, Beijing 100081, China

Pingbing Ming
LSEC, ICMSEC, Academy of Mathematics and Systems Science, Chinese Academy of Sciences, Beijing 100080, China

Ju Li*
Department of Materials Science and Engineering, Ohio State University, Columbus, Ohio 43210, USA
(Received 14 May 2007; revised manuscript received 16 June 2007; published 28 August 2007)

Graphene-based sp^2-carbon nanostructures such as carbon nanotubes and nanofibers can fail near their ideal strengths due to their exceedingly small dimensions. We have calculated the phonon spectra of graphene as a function of uniaxial tension by density functional perturbation theory to assess the first occurrence of phonon instability on the strain path, which controls the strength of a defect-free crystal at 0 K. Uniaxial tensile strain is applied in the x (nearest-neighbor) and y (second nearest-neighbor) directions, related to tensile deformation of zigzag and armchair nanotubes, respectively. The Young's modulus $E=1050$ GPa and Poisson's ratio $\nu=0.186$ from our small-strain results are in good agreement with previous calculations. We find that in both x and y uniaxial tensions, phonon instabilities occur near the center of the Brillouin zone, at ($\varepsilon_{xx}=0.194$, $\sigma_{xx}=110$ GPa, $\varepsilon_{yy}=-0.016$) and ($\varepsilon_{yy}=0.266$, $\sigma_{yy}=121$ GPa, $\varepsilon_{xx}=-0.027$), respectively. Both soft phonons are longitudinal elastic waves in the pulling direction, suggesting that brittle cleavage fracture may be an inherent behavior of graphene and carbon nanotubes at low temperatures. We also predict that a phonon band gap will appear in highly stretched graphene, which could be a useful spectroscopic signature for highly stressed carbon nanotubes.

DOI: 10.1103/PhysRevB.76.064120 PACS number(s): 63.20.Dj, 62.20.−x, 81.05.Uw, 81.07.De

I. MOTIVATION

The ideal strength[1,2] is the highest achievable strength of a defect-free crystal at 0 K. Even though a conventional material deforms or fractures at macroscopic stresses far below its ideal strength, the ideal strength is nonetheless a crucial theoretical parameter, because it fundamentally characterizes the nature of chemical bonding in that crystal.[3,4] The Peierls-Nabarro model of dislocation,[5,6] for instance, relies on the Frenkel model of ideal strength, because defects such as cracks and dislocations work like levers, amplifying the far-field stress to near ideal strength levels inside the defect core in order to move.[7] It is thus not surprising that the study of ideal strength can tell us a lot about why some materials (such as diamond) are intrinsically brittle, while others (such as copper) are intrinsically ductile.[4]

The ideal strength becomes even more important with the progress of nanotechnology. Recent experiments on nanocrystals,[8] nanoporous materials,[9] nanopillars,[10] and nanoindentation[11] have revealed a host of *ultrastrength* phenomena, defined by internal stress levels broadly and persistently rising up to a significant fraction of the ideal strength. Ultrastrength materials typically have geometric features around or less than $L_C \sim 10^2$ nm. To put this in perspective, computers one can buy off the shelf now have chips with 65 nm strained silicon features.[12] At such material length scales, the population dynamics of defects is fundamentally different from that in the macroscale material, leading to size-dependent mechanical behavior at $L > L_C$, which, however, starts to level off at $L < L_C$ due to the intrinsic upper bound, the ideal strength.

Carbon nanotube is an ultimate example of small-size, ultrastrength material. By bending multiwalled carbon nanotubes (MWCNTs) inside an atomic force microscope, Falvo *et al.* estimated that 16% tensile strain can be achieved in local regions of some MWCNTs without breaking them.[13] Yu *et al.* measured the tensile response of single-walled carbon nanotube (SWCNT) ropes[14] and inferred a mean breaking strength of 30 GPa, 3% of their mean Young's modulus of 1002 GPa. Ding *et al.*[15] measured the fracture strengths and moduli of arc-grown MWCNTs. The outer-shell fracture strength was estimated to range from 10 to 66 GPa, and the Young's modulus from 620 to 1200 GPa. Demczyk *et al.* conducted room-temperature pulling and bending tests on MWCNT of diameter of 12.5 nm and measured an astonishing 150 GPa failure strength, which is 17% of its Young's modulus, $E=900$ GPa.[16] The authors noted there is no narrowing of the nanotubes immediately before failure (the deformation was elastic and reversible), and the nanotubes fail "as essentially defect-free materials." The 150 GPa strength value, however, seems to be inconsistent with their reported 5% strain prior to failure. Barber *et al.*[17] measured the tensile strength of MWCNTs produced by chemical vapor deposition and fitted the data to the Weibull-Poisson distribution. A characteristic strength value of 109 GPa was obtained. Márquez-Lucero *et al.* reported similar high strengths in carbon nanotubes and nanofibers.[18] These recent experiments indicate that *ultratensile* strength can indeed be achieved in an important component of nanotechnology.

It is reasonable to speculate that graphene-based carbon nanotubes, nanofibers, etc., hold record or near-record ideal tensile strength among all materials. It is well known that the electronic structure and mechanical properties of carbon nanotubes are similar to those of flat graphene, aside from quantum confinement effect.[19] For this paper

 ©2007 The American Physical Society

we perform a careful *ab initio* study of the ideal tensile strength of flat graphene as structural motif for carbon nanotubes, nanofibers, and other graphene-based materials.[20] The results we obtain for the ideal strain ε_I and ideal strength σ_I are expected to be directly comparable with experimental measurements for the carbon nanotubes.[13–17]

II. METHODOLOGY

The ideal strength σ_I of a crystal is inherently related to its phonons.[21,22] This is because at low temperatures (defined here as less than half the Debye temperature T_D, $T_D \sim 1000$ K in graphene[23]), all atomic motions in the crystal can be decomposed into phonon modes, which are nearly independent of each other (normal modes). Therefore, the both necessary and sufficient condition for mechanical instability of a crystal at low temperature is phonon instability,[24,25] i.e., vanishing of the phonon frequency $\omega_{n\mathbf{k}}$ for some wave vector $\mathbf{k}$ and branch index n. A mathematical understanding of this condition and its relation to the validity of the Cauchy-Born rule relating stress to strain can be found in Ref. 26. A phonon mode that lowers the energy of a crystal (has imaginary frequency) will grow in amplitude, until nonlinearity kicks in and the structure is driven to a new stable state, often containing strain-relieving defects.[25] The incremental atomic displacements of the unstable phonon mode can be determined from the eigenvectors of the dynamical matrix. The unstable eigenvector indicates the crystallographic nature of the initial instability. When free surfaces are under load, the so-called surface ideal strength[27,28] can also be calculated from surface phonon analysis.[29]

Density functional perturbation theory (DFPT) is a well-tested *ab initio* method for accurate phonon calculations.[30] Typical empirical interatomic potentials for semiconductors give up to 20% error in the calculated phonon frequencies at zero stress compared to experiments,[31] but one could usually expect $<5\%$ error from parameter-free DFPT calculations.[30] Furthermore, empirical interatomic potentials are fitted to mostly zero-stress properties; large-strain atomic environments leading to nonlinearity and bond breaking are often under-represented in the fitting process. Therefore, empirical potential phonon calculations[24,29] are useful for surveying the gross features of ideal strength but are inappropriate for accurate predictions of ideal strength. The DFPT approach, on the other hand, does not have this problem. One can expect a similar level of accuracy at zero stress as at large stress.

DFPT calculations of phonon instabilities and ideal strength have been performed for Al (Ref. 32) and Si.[33] Recently, there have been a number of experimental[34,35] and theoretical[36,37] studies of phonon dispersion in graphene, which affirmed the accuracy of the DFPT approach. However, none have dealt with the ideal strength connection.

We performed our calculations using the plane wave density functional theory (DFT) program ABINIT,[38] within local density approximation (LDA). The Troullier-Martins norm-conserving pseudopotential[39] was used for carbon, with a plane wave kinetic energy cutoff of 1633 eV. The stress-strain calculations are performed in the four-atom unit cell, shown in Fig. 1(a). The supercell height $Z=8$ Å in the z direction is much larger than the interlayer spacing of $d_0 = 3.34$ Å in graphite[40] and carbon nanotubes. Brillouin zone (BZ) integration for charge density and total energy is performed with a 10×18 Monkhorst-Pack grid. We employ 0.1 eV Fermi-Dirac smearing of the occupation number around the Fermi level. Convergence studies indicate that the error in the stresses and energy due to the basis set size, smearing parameter, and $\mathbf{k}$-point grid density is less than 0.1 GPa and 0.5 meV, respectively. We first optimized the equilibrium carbon-carbon distance by the Broyden-Fletcher-Goldfarb-Shanno method and obtained a value of $R_{CC} = 1.4148$ Å, which is only slightly different ($\leqslant 0.5\%$) from the experimental value of 1.419 Å.[40]

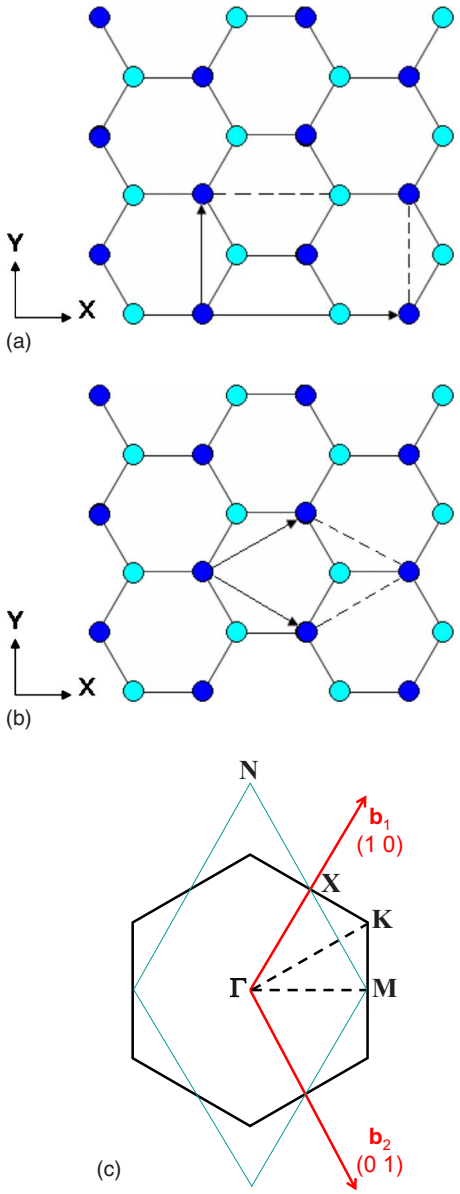

FIG. 1. (Color online) (a) Four-atom unit cell for stress-strain calculations. (b) Two-atom primitive cell for phonon calculations. (c) Primitive cell of the reciprocal lattice and the first Brillouin zone.

Figure 1(c) shows the reciprocal lattice of graphene sheet and its first Brillouin zone. For the DFPT phonon calcula-

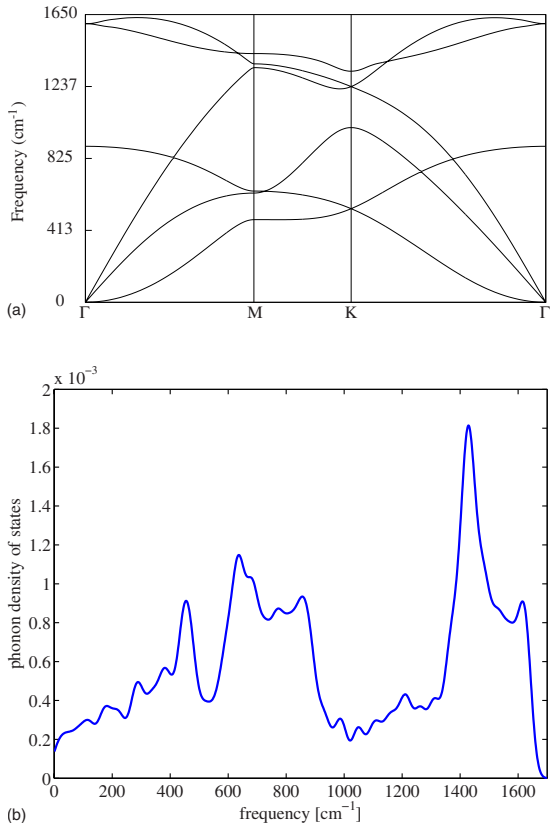

FIG. 2. (Color online) DFPT calculated (a) phonon dispersion and (b) density of states of graphene sheet at zero stress. Note that the free bending wave $\omega^2=\kappa k^4$ near Γ in (a) introduces a finite density of states at zero frequency in (b).

tions, we used a two-atom primitive cell [Fig. 1(b)] and a 20×20 **k** grid to map out all the possible instabilities. The results at zero stress along Γ-M-K-Γ are shown in Fig. 2(a). Our results are almost identical to those of Dubay and Kresse[36] and Wirtz and Rubio.[37] The lowest branch near Γ, $\omega^2=\kappa k^4$, describes free bending wave of the graphene sheet at zero stress, where κ is proportional to the bending modulus of the sheet. Such free bending wave is absent in three-dimensional crystals. It introduces a finite density of states at zero frequency, as shown in Fig. 2(b). According to shell elasticity, under a finite tensile stress $\sigma>0$, this bending wave branch will turn into $\omega^2=\kappa k^4+\lambda\sigma k^2$ near Γ, thus no longer looking fundamentally different from the other phonon branches. So, under a nonzero tensile stress, we would expect the phonon density of states to approach 0 as the frequency $\rightarrow 0$.

We then apply a series of incremental tensile strains on the supercell and simultaneously relax the other stress components to zero (Poisson contraction under uniaxial tension). Uniaxial tension was applied in the x direction and y direction (Fig. 1), respectively. The x direction is the nearest-neighbor C-C bonding direction. Pulling in the x direction corresponds to pulling a zigzag nanotube of chirality $(n,0)$, and the Poisson effect corresponds to elastic shrinking of the circumferential length of the zigzag nanotube in tension. The y direction is the second-nearest-neighbor direction. Pulling

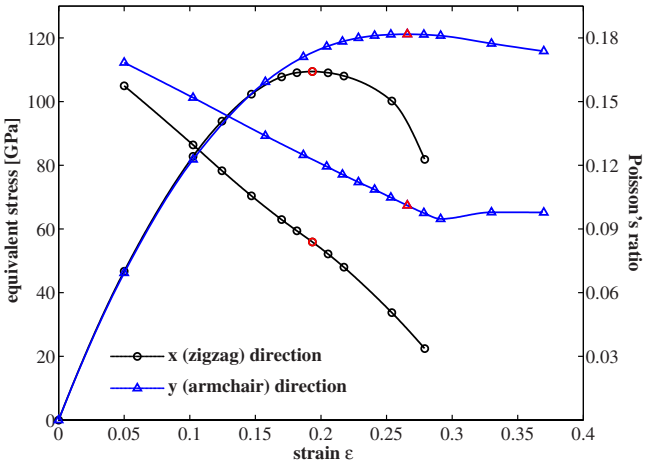

FIG. 3. (Color online) The curves connected to the origin are the equivalent tensile stress ($d_0=3.34$ Å) versus uniaxial strain in the x and y directions, respectively. The lines with initially negative slopes (scale labels to the right) are the finite-deformation Poisson's ratios as functions of the uniaxial strain in the x and y directions, respectively. The red circles and triangles indicate the condition where peak stress could be attained for zigzag and armchair nanotubes, respectively.

in the y direction corresponds to pulling an armchair nanotube of chirality (n,n), and the Poisson effect then corresponds to elastic shrinking of the armchair nanotube diameter under tension. Since the graphene primitive cell contains two atoms, there is an additional internal relative displacement beyond the affine displacements, and the Hellmann-Feynman forces need to be relaxed to zero at every strain.

Here, we want to make a distinction between the calculated *supercell stress* and *equivalent stress*. The equilibrium interlayer spacing $d_0=3.34$ Å of graphite and carbon nanotubes in nature is established through van der Waals interactions, which have minimal effect on the in-plane covalent carbon-carbon interactions. However, LDA is known to have artifacts treating the weak van der Waals interactions. Therefore, in our calculations, we have artificially set the supercell height to $Z=8$ Å. The supercell stress computed from ABINIT is derived from linear response theory in the same vein as DFPT[41] and is by default averaged over the entire supercell volume. To make connections with experiments[16] and other calculations,[42–44] however, we need to rescale the supercell stress by Z/d_0 to obtain the equivalent stress. The idea is that graphene should be nominally considered a continuum plate of constant thickness d_0 (with no Poisson's contraction in the z direction) in the context of continuum mechanics. Thus, a SWCNT is by convention regarded as a hollow pipe rather than a full cylinder. This convention is significant when discussing the bending and buckling behavior of SWCNT,[45] as well as the mechanics of MWCNT.[16]

Previous plane wave DFT calculation by Ogata and Shibutani[46] indicated that peak stress of 107.4 GPa may be achieved in (10,0) zigzag SWCNT at a critical strain of 0.208, and peak stress of 114.6 GPa may be achieved in (8,8) armchair SWCNT at a critical strain of 0.295 if the nanotube could maintain its lattice structure on the strain paths. Be-

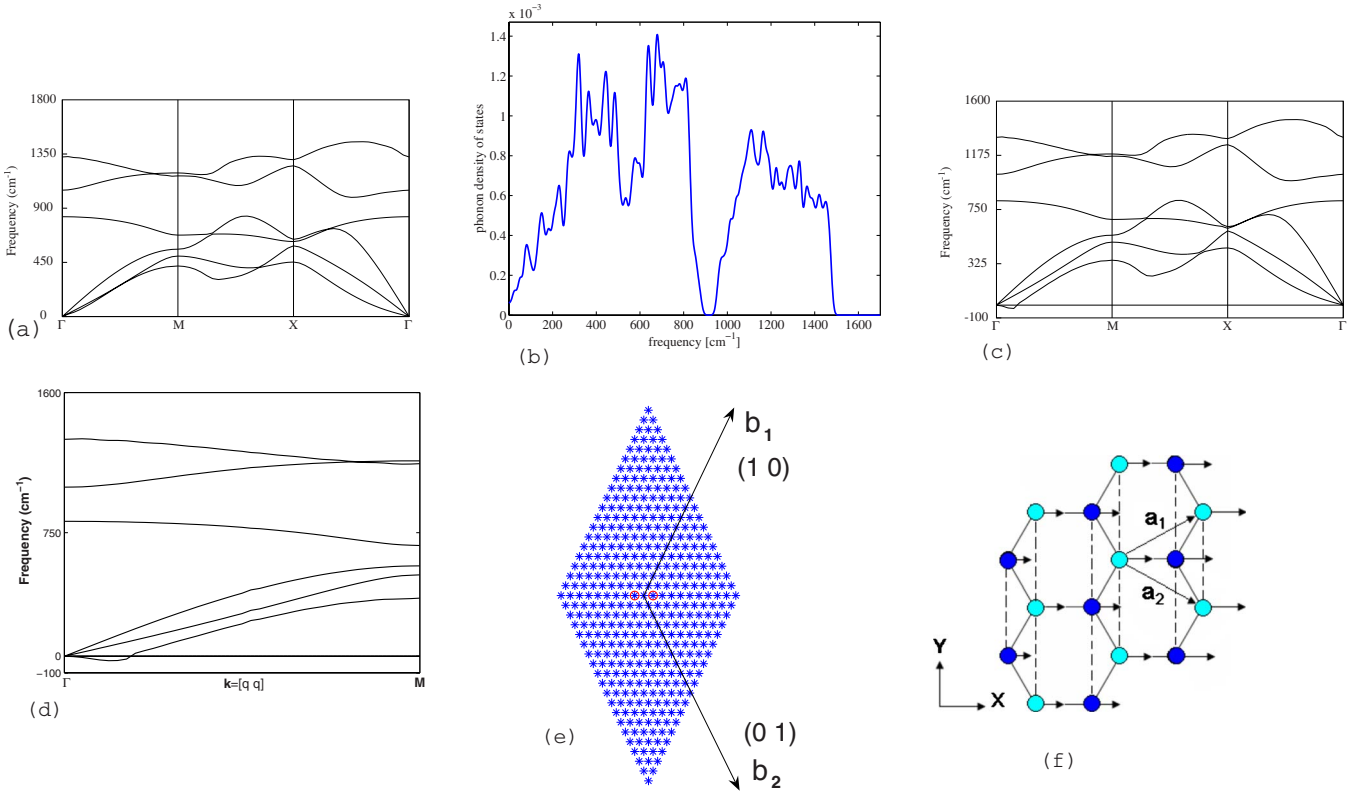

FIG. 4. (Color online) (a) Phonon dispersion and (b) density of states of graphene at $\varepsilon_{xx}=0.18$. There is no soft mode yet. (c) Phonon dispersion at $\varepsilon_{xx}=0.194$, $\sigma_{xx}=110$ GPa. (d) Blow-up of the unstable branch along $\mathbf{k}=q(\mathbf{b}_1+\mathbf{b}_2)=k\mathbf{e}_x$. (e) Scan of the entire Brillouin zone at $\varepsilon_{xx}=0.194$ to make sure that (d) is the first phonon instability. ⊛ indicates imaginary frequency and * indicates real frequency. (f) The unstable eigenvector corresponding to the soft mode at $\varepsilon_{xx}=0.194$.

cause only a single unit cell was employed in the nanotube axis direction, the calculation was not able to detect any $\mathbf{k}\neq 0$ phonon instability. Mielke *et al.*[47] and Khare *et al.*[48] performed semiempirical quantum mechanical calculations (PM3) with larger numbers of atoms. They predicted failure stress of 124 GPa at a critical strain of 0.20 for (10,0) zigzag SWCNT and failure stress of 135 GPa at a critical strain of 0.30 for (5,5) armchair SWCNT, respectively. Such calculations can potentially capture $\mathbf{k}\neq 0$ phonon instability. However, the results were not analyzed this way.

III. RESULTS AND DISCUSSIONS

Figure 3 shows the DFT calculated stress-strain curve and finite-deformation Poisson's ratio of graphene. Here, strain is defined as $\varepsilon\equiv L/L_0-1$, and stress σ is the Cauchy stress,[49] assuming that the nominal plate thickness $d_0=3.34$ Å is independent of ε. The finite-deformation Poisson's ratio is defined as $\nu\equiv-\varepsilon(\text{lateral})/\varepsilon(\text{pulling})$, where ε(lateral) is the in-plane shrinkage perpendicular to the pulling axis. At small strains, graphene has isotropic in-plane elastic response, with Young's modulus $E=1050$ GPa and Poisson's ratio $\nu=0.186$ assessed from our DFT-LDA results. These are in good agreement with previous DFT calculations.[50] At large strains, the lattice symmetry is broken, and the x-strain elastic response becomes distinct from the y-strain elastic response.

The function $\nu(\varepsilon)$ has a noticeable downward trend at large strain, indicating gradual saturation of the amount of Poisson contraction. The maximum Cauchy stress for uniaxial tension in x (relevant for zigzag nanotubes) is 110 GPa, at $\varepsilon_{xx}=0.194$, $\varepsilon_{yy}=-0.016$. Thus, we should expect no more than 1.6% shrinkage in the zigzag nanotube diameter when pulled to failure at low temperatures, in agreement with experimental observations.[16] The predicted peak strength is in reasonable agreement with the earlier DFT estimate of 107.4 GPa at critical strain of 0.208 for a zigzag nanotube.[46]

Compared to being pulled in the x direction, graphene is somewhat stronger in the y direction (relevant for armchair nanotubes), with maximum Cauchy stress of 121 GPa, at $\varepsilon_{yy}=0.266$, $\varepsilon_{xx}=-0.027$. Thus, we predict the armchair nanotubes to be 10% stronger than the zigzag nanotubes and can withstand 37% larger strain, with maximum diameter contraction of 2.7% (elastic) before failure at low temperatures. This peak strength is consistent with the earlier DFT estimate of 114.6 GPa at critical strain of 0.295 for an armchair nanotube.[46]

While Fig. 3 provides a rough indication of the low-temperature strength of graphene-based nanostructures, they do not theoretically *guarantee* that the peak stresses can be *attained*, because finite-$\mathbf{k}$ phonon instabilities could intervene on the strain path and disrupt the homogeneous lattice structure before the peak stress is ever achieved (the instability is not soft elastic wave in nature[24]). For instance, Clat-

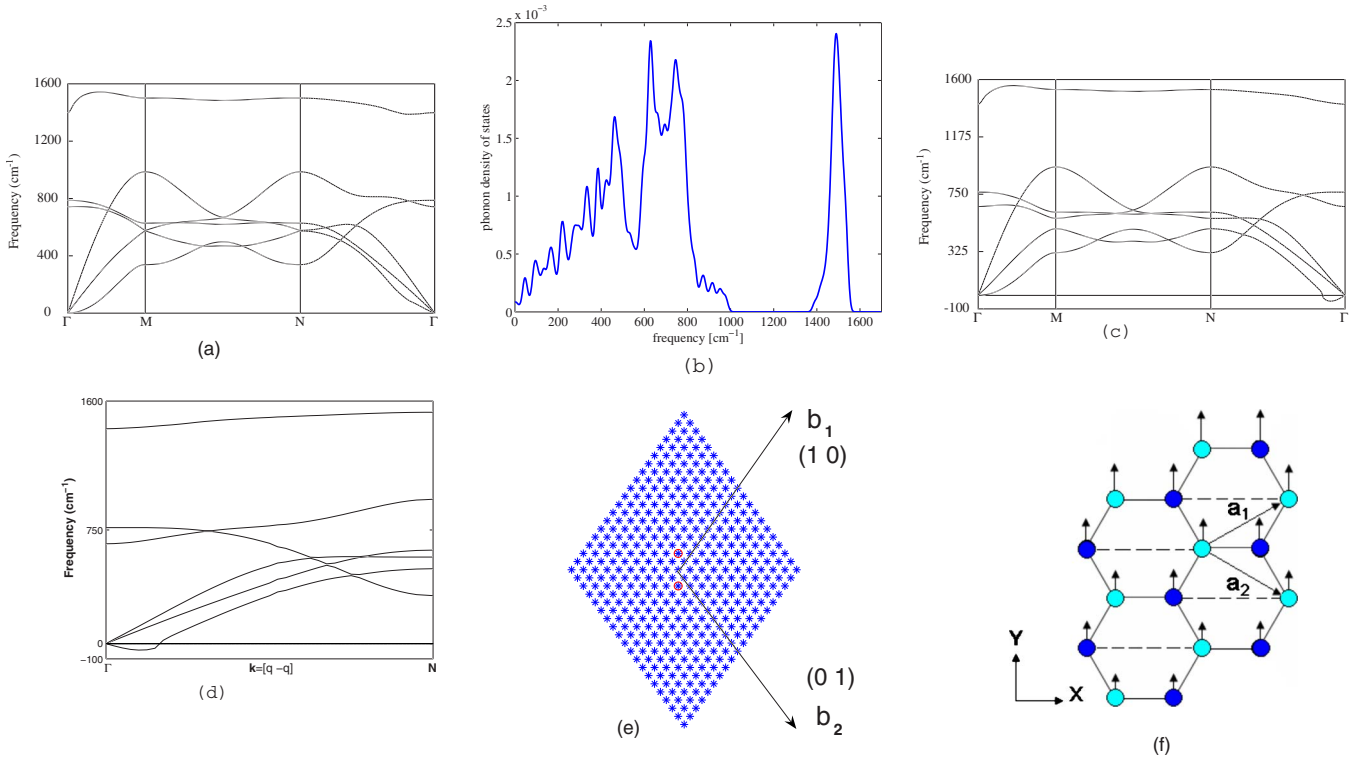

FIG. 5. (Color online) (a) Phonon dispersion and (b) density of states of graphene at $\varepsilon_{yy}=0.24$. There is no soft mode yet. (c) Phonon dispersion at $\varepsilon_{yy}=0.266$, $\sigma_{yy}=121$ GPa. (d) Blow-up of the unstable branch along $\mathbf{k}=q(\mathbf{b}_1-\mathbf{b}_2)=k\mathbf{e}_y$. (e) Scan of the entire Brillouin zone at $\varepsilon_{yy}=0.266$ to make sure (d) is the first phonon instability. ⊛ indicates imaginary frequency and * indicates real frequency. (f) The unstable eigenvector corresponding to the soft mode at $\varepsilon_{yy}=0.266$.

terbuck *et al.* showed that in face-centered-cubic aluminum, under ⟨110⟩, ⟨100⟩, ⟨111⟩ uniaxial tension, as well as relaxed $\langle 11\bar{2}\rangle$ {111} shear, the onset of finite-**k** phonon instabilities all occur *before* the peak stress. It is, therefore, imperative for us to check the stability of all phonons on the strain path using the DFPT phonon calculations. We take the "carpet bombing" approach, that is to say, we check all **k** points in the irreducible BZ on a two-dimensional grid.

The results for uniaxial tension in x are shown in Fig. 4. At $\varepsilon_{xx}=0.18$, there is no indication of phonon instability [Fig. 4(a)], that is, all of the phonon frequencies shown are positive, but significant phonon softening (lowering of the frequencies) has occurred compared to Fig. 2, except for the bending wave branch which stiffens in tension. Also, as shown in Fig. 4(b) a narrow phonon band gap appears around 900 cm^{-1}, which might be a useful signature to spectroscopically determine highly stressed carbon nanotubes.

Figure 4(c) indicates that phonon instability does occur at $\varepsilon_{xx}=0.194$, $\sigma_{xx}=110$ GPa, along the $\mathbf{k}=q(\mathbf{b}_1+\mathbf{b}_2)=k\mathbf{e}_x$ direction. Blow-up view [Fig. 4(d)] indicates that the instability is of long-wave nature, near Γ. The initial slope of the dispersion curve is imaginary. When this happens, the material is unstable with respect to incremental tensile strain and is thus elastically unstable. To make sure this long wave at $\varepsilon_{xx}=0.194$ is the first instance of phonon instability on the strain path, Fig. 4(e) shows the entire Brillouin zone instead of just the selected cuts. All phonon frequencies on the two-dimensional grid are positive, except for the two grid points near the zone center. Thus, the first instability is elastic in nature, which means that the peak stress and strain can be attained at 0 K, $\sigma_{I,xx}=110$ GPa, $\varepsilon_{I,xx}=0.194$.

For such situation, a general theory exists about how a linear instability of long waves can lead to dynamic nucleation of defect singularities such as dislocations or cracks.[24,25] In simple crystals, if **w** is more perpendicular to **k**, then the unstable wave is transversal, i.e., it is a soft shear wave. It is very likely then that a dislocation loop or a twin embryo would be nucleated. If, however, **w** is more parallel to **k**, then the unstable wave is longitudinal, and a microcrack is likely to result.

The eigenvector of the dynamical matrix [Fig. 4(f)] indicates that this soft phonon mode at $\varepsilon_{I,xx}=0.194$ is a longitudinal wave, with polarization displacement **w** parallel to $\mathbf{k}\|\mathbf{e}_x$, and thus should lead to the nucleation of microcrack when $\sigma_{I,xx}=110$ GPa is attained at $T=0$ K. This is in agreement with the analysis of Dumitrica *et al.*[43] that at low temperatures, the failure mode of zigzag nanotubes is brittle cleavage fracture. Only when the temperature is high enough ($T>T_D/2\sim 500$ K) can zigzag nanotubes deform plastically at laboratory strain rates via the nucleation and migration of Stone-Wales 5/7 defects.[43,45] At such elevated temperatures, the ideal strength (athermal strength) is no longer a good indicator of the prevalent deformation mechanism; one must also look at thermally activated processes and their activation volumes,[7,28,51] which is beyond the scope of this paper.

The DFPT phonon calculations for uniaxial tension in y (armchair nanotubes) are shown in Fig. 5. The results are similar to uniaxial tension in x, except that the phonon band gap is now much wider. This gap centered around 1200 cm^{-1}

would be a good diagnostic signature of highly stressed carbon nanotubes. We predict longitudinal elastic wave instability for armchair nanotubes, with $\mathbf{w}\|\mathbf{k}\|\mathbf{e}_y$, at $\varepsilon_{I,yy}=0.266$ and $\sigma_{I,yy}=121$ GPa, which usually suggests brittle cleavage fracture behavior.[25] Analysis of the relationship between $\mathbf{w}$ and atomic geometry [Fig. 5(f)], however, reveals a small difference. While $\mathbf{w}$ was parallel to the highest-load nearest-neighbor bonds in Fig. 4(f), it now has an $\sim 30°$ angle to the highest-load bonds in Fig. 5(f). This means that in a longitudinal displacement field like $\mathbf{u}(\mathbf{x})=\mathbf{w}e^{i\mathbf{k}\cdot\mathbf{x}}$, while the highest-load bonds in Fig. 4(f) sustain stretching but not rotation, the highest-load bonds will sustain both bond stretching and bond rotation in Fig. 5(f). Because the Stone-Wales transformation involves bond rotation,[45] it is not absolutely clear whether the linear instability of Fig. 5(f) will lead to bond cleavage first or localized Stone-Wales transformation first. Such complication arises because graphene has a two-atom primitive cell and the response to macroscopic strain is nonaffine.

Dumitrica *et al.* predicted localized Stone-Wales transformation and plastic deformation for armchair nanotubes at low temperatures[43] ($T=1$, 300, and 600 K) in a stress ramp-up experiment. We note that experimentally, there is no evidence yet of low-temperature plastic deformation of carbon nanotubes of any chirality. Demczyk *et al.* found no plastic narrowing of the nanotubes immediately before failure.[16] On the other hand, it is possible to fracture quickly (with respect to human time scale) after the 5/7 defects have been nucleated[52] or perhaps after the aggregation of several 5/7 defects.[53] Thus, experiments to date provide no concrete evidence either for or against initial Stone-Wales transformation at low temperature and laboratory strain rates. It is reasonable, however, to interpret our DFPT results as suggesting that both the zigzag and armchair nanotubes are intrinsically capable of brittle cleavage fracture at $T=0$ K due to the longitudinal elastic wave nature of the first soft phonons when subjected to tension.

ACKNOWLEDGMENTS

F.L. acknowledges support from the National Natural Science Foundation of China (10425105) and the Chinese National Basic Research Program (2005CB321704). The calculations were performed on LSSC-II at the State Key Laboratory of Scientific and Engineering Computing, Chinese Academy of Sciences. P.M. acknowledges support under the National Natural Science Foundation of China (10571172) and the Chinese National Basic Research Program (2005CB321704). J.L. acknowledges support by DoE DE-FG02-06ER46330, NSF DMR-0502711, ONR N00014-05-1-0504, AFOSR, and Ohio Supercomputer Center.

*li.562@osu.edu

[1] T. Li, J. W. Morris, Jr., N. Nagasako, S. Kuramoto, and D. C. Chrzan, Phys. Rev. Lett. **98**, 105503 (2007).
[2] J. Pokluda, M. Černý, P. Šandera, and M. Šob, J. Comput.-Aided Mater. Des. **11**, 1 (2004).
[3] S. Ogata, J. Li, and S. Yip, Science **298**, 807 (2002).
[4] S. Ogata, J. Li, N. Hirosaki, Y. Shibutani, and S. Yip, Phys. Rev. B **70**, 104104 (2004).
[5] R. Peierls, Proc. Phys. Soc. London **52**, 34 (1940).
[6] F. R. N. Nabarro, Proc. Phys. Soc. London **59**, 256 (1947).
[7] J. Li, MRS Bull. **32**, 151 (2007).
[8] K. S. Kumar, H. Van Swygenhoven, and S. Suresh, Acta Mater. **51**, 5743 (2003).
[9] C. A. Volkert, E. T. Lilleodden, D. Kramer, and J. Weissmüller, Appl. Phys. Lett. **89**, 061920 (2006).
[10] J. R. Greer and W. D. Nix, Phys. Rev. B **73**, 245410 (2006).
[11] A. Gouldstone, N. Chollacoop, M. Dao, J. Li, A. M. Minor, and Y.-L. Shen, Acta Mater. **55**, 4015 (2007).
[12] P. R. Chidambaram, C. Bowen, S. Chakravarthi, C. Machala, and R. Wise, IEEE Trans. Electron Devices **53**, 944 (2006).
[13] M. R. Falvo, G. J. Clary, R. M. Taylor II, V. Chi, F. P. Brooks, Jr., S. Washburn, and R. Superfine, Nature (London) **389**, 582 (1997).
[14] M. F. Yu, B. S. Files, S. Arepalli, and R. S. Ruoff, Phys. Rev. Lett. **84**, 5552 (2000).
[15] W. Ding, L. Calabri, K. M. Kohlhaas, X. Chen, D. A. Dikin, and R. S. Ruoff, Exp. Mech. **47**, 25 (2007).
[16] B. G. Demczyk, Y. M. Wang, J. Cumings, M. Hetman, W. Han, A. Zettl, and R. O. Ritchie, Mater. Sci. Eng., A **334**, 173 (2002).
[17] A. H. Barber, R. Andrews, L. S. Schadler, and H. D. Wagner, Appl. Phys. Lett. **87**, 203106 (2005).
[18] A. Márquez-Lucero, J. A. Gomez, R. Caudillo, M. Miki-Yoshida, and M. José-Yacaman, Small **1**, 640 (2005).
[19] R. Saito, G. Dresselhaus, and M. S. Dresselhaus, *Physical Properties of Carbon Nanotubes* (Imperial College Press, London, 1998).
[20] S. Stankovich, D. A. Dikin, G. H. B. Dommett, K. M. Kohlhaas, E. J. Zimney, E. A. Stach, R. D. Piner, S. T. Nguyen, and R. S. Ruoff, Nature (London) **442**, 282 (2006).
[21] M. T. Dove, *Introduction to Lattice Dynamics* (Cambridge University Press, Cambridge, 1993).
[22] A. Maradudin, E. Montroll, G. Weiss, and I. Ipatova, *Theory of Lattice Dynamics in the Harmonic Approximation*, 2nd ed. (Academic Press, New York, 1971).
[23] T. Tohei, A. Kuwabara, F. Oba, and I. Tanaka, Phys. Rev. B **73**, 064304 (2006).
[24] J. Li and S. Yip, Comput. Model. Eng. Sci. **3**, 219 (2002).
[25] J. Li, A. H. W. Ngan, and P. Gumbsch, Acta Mater. **51**, 5711 (2003).
[26] W. N. E. and P. B. Ming, Arch. Ration. Mech. Anal. **183**, 241 (2007).
[27] Y. Umeno, A. Kushima, T. Kitamura, P. Gumbsch, and J. Li, Phys. Rev. B **72**, 165431 (2005).
[28] T. Zhu, J. Li, A. Samanta, A. Leach, and K. Gall (unpublished).
[29] S. V. Dmitriev, T. Kitamura, J. Li, Y. Umeno, K. Yashiro, and N. Yoshikawa, Acta Mater. **53**, 1215 (2005).
[30] S. Baroni, S. de Gironcoli, A. Dal Corso, and P. Giannozzi, Rev. Mod. Phys. **73**, 515 (2001).

[31] L. J. Porter, J. Li, and S. Yip, J. Nucl. Mater. **246**, 53 (1997).
[32] D. M. Clatterbuck, C. R. Krenn, M. L. Cohen, and J. W. Morris, Jr., Phys. Rev. Lett. **91**, 135501 (2003).
[33] S. M.-M. Dubois, G.-M. Rignanese, T. Pardoen, and J.-C. Charlier, Phys. Rev. B **74**, 235203 (2006).
[34] A. Grüneis, R. Saito, T. Kimura, L. G. Cancado, M. A. Pimenta, A. Jorio, A. G. Souza Filho, G. Dresselhaus, and M. S. Dresselhaus, Phys. Rev. B **65**, 155405 (2002).
[35] J. Maultzsch, S. Reich, C. Thomsen, H. Requardt, and P. Ordejón, Phys. Rev. Lett. **92**, 075501 (2004).
[36] O. Dubay and G. Kresse, Phys. Rev. B **67**, 035401 (2003).
[37] L. Wirtz and A. Rubio, Solid State Commun. **131**, 141 (2004).
[38] X. Gonze *et al.*, Comput. Mater. Sci. **25**, 478 (2002).
[39] N. Troullier and J. L. Martins, Phys. Rev. B **43**, 1993 (1991).
[40] Y. Baskin and L. Meyer, Phys. Rev. **100**, 544 (1955).
[41] R. M. Martin, *Electronic Structure: Basic Theory and Practical Methods* (Cambridge University Press, Cambridge, 2004).
[42] T. Dumitrică, T. Belytschko, and B. I. Yakobson, J. Chem. Phys. **118**, 9485 (2003).
[43] T. Dumitrica, M. Hua, and B. I. Yakobson, Proc. Natl. Acad. Sci. U.S.A. **103**, 6105 (2006).
[44] P. W. Chung, Phys. Rev. B **73**, 075433 (2006).
[45] H. Mori, S. Ogata, J. Li, S. Akita, and Y. Nakayama, Phys. Rev. B **74**, 165418 (2006).
[46] S. Ogata and Y. Shibutani, Phys. Rev. B **68**, 165409 (2003).
[47] S. L. Mielke, D. Troya, S. Zhang, J.-L. Li, S. P. Xiao, R. Car, R. S. Ruoff, G. C. Schatz, and T. Belytschko, Chem. Phys. Lett. **390**, 413 (2004).
[48] R. Khare, S. L. Mielke, J. T. Paci, S. L. Zhang, R. Ballarini, G. C. Schatz, and T. Belytschko, Phys. Rev. B **75**, 075412 (2007).
[49] T. Zhu, J. Li, K. J. Van Vliet, S. Ogata, S. Yip, and S. Suresh, J. Mech. Phys. Solids **52**, 691 (2004).
[50] K. N. Kudin, G. E. Scuseria, and B. I. Yakobson, Phys. Rev. B **64**, 235406 (2001).
[51] T. Zhu, J. Li, A. Samanta, H. G. Kim, and S. Suresh, Proc. Natl. Acad. Sci. U.S.A. **104**, 3031 (2007).
[52] J. Song, H. Jiang, D.-L. Shi, X.-Q. Feng, Y. Huang, M.-F. Yu, and K.-C. Hwang, Int. J. Mech. Sci. **48**, 1464 (2006).
[53] D. Troya, S. L. Mielke, and G. C. Schatz, Chem. Phys. Lett. **382**, 133 (2003).